1. Molecular Mechanism of Surface Recognition. Azo Dyes Degradation on Fe, Ti, and Al Oxides through Metal Sulfonate Complexes

ARTICLE *in* LANGMUIR · SEPTEMBER 1999

Impact Factor: 4.46 · DOI: 10.1021/la9900270

3 AUTHORS:

Jayasundera Bandara
National Institute of Fundamental Studies - S…
91 PUBLICATIONS **2,641** CITATIONS
SEE PROFILE

Jerzy A Mielczarski
University of Lorraine
58 PUBLICATIONS **1,684** CITATIONS
SEE PROFILE

J. Kiwi
École Polytechnique Fédérale de Lausanne
328 PUBLICATIONS **10,953** CITATIONS
SEE PROFILE

1. Molecular Mechanism of Surface Recognition. Azo Dyes Degradation on Fe, Ti, and Al Oxides through Metal Sulfonate Complexes

J. Bandara,[†] J. A. Mielczarski,[‡] and J. Kiwi*,[†]

Department of Chemistry, Institute of Physical Chemistry, Swiss Federal Institute of Technology, 1015 Lausanne, Switzerland, and Laboratoire LEM/UMR 7569 CNRS, INPL-ENSG, BP 40, 54501 Vandoeuvre-les-Nancy Cedex, France

Received January 11, 1999. In Final Form: June 24, 1999

The adsorption of azo dyes (Orange II, Orange I, and Orange G) on α-Fe_2O_3 and α-FeOOH has been carried out, and the results are compared with those for adsorption on TiO_2 and Al_2O_3. Adsorption of azo dye was less favored when the sulfonic groups were on the naphthalene ring, as in the case of Orange G, suggesting an inner sphere mechanism of complex formation between the dye and α-Fe_2O_3. The crystalline face of the oxide and the appropriate metal−metal atomic distance rather than the density of surface sites (surface area) seem to control the extent of the adsorption. The latter observations imply a surface molecular recognition mechanism active during the adsorption process of different azo dyes on the particular oxide surface. The adsorption of Orange II (taken as a model dye) from solution at pH ≤ 7 could be understood in electrostatic terms taking into account the species found at the surface of the oxides and the Orange II ionization as a function of solution pH. Modeling of the adsorption processes was carried out taking into account the number of adsorption sites, the equilibria constants, and the surface area of the different azo dyes. The most favorable condition for adsorption was the closest matching of the M−M atomic distance of the oxide to the O−O bond distance in the sulfonic group: −O−S−(O−O) of Orange II. The adsorption of azo dyes was found to occur via the sulfonic group of Orange II through the formation of a bridged bidentate complex. A variety of techniques have been used to follow the adsorption, such as diffuse reflectance infrared fourier transform spectroscopy (DRIFT), high-pressure liquid chromatography (HPLC), surface zeta potential (ζ), UV−vis spectrophotometry, and N_2 (BET) adsorption.

Introduction

The degradation of azo dyes such as Orange I, II, and G on heterogeneous particulate material is commonly preceded by adsorption on the substrate as a precursor step to the abatement of these compounds.[1−5] The adsorption ability of the hematite arises from the surface hydroxyl groups' intervention during dissociative chemisorption of the adsorbate.

Synthetic textile dyes of the azo family represent an important part of the world production of synthetic dyes and are characterized by the presence of the azo group (−N═N−).[5−7] Azo dyes released without proper treatment represents about 15% of the total world production, that is, 150 tons per day. Most of the azo dye compounds are resistant to bacterial activity, and therefore, biological treatment alone cannot be used to remove them from effluents within acceptable time periods. Azo dyes reduce under anaerobic conditions, and the reaction products lead to hazardous aromatic amines.[8] Work related to the sensitized degradation of azo dyes[9] describes the charge transfer between the dye and the substrate as determined by the way the molecule contacts the oxide surface, that is, whether it forms a strong surface complex[10] or just adsorbs on the substrate via weak physical attraction forces.[11,12] The most important factors controlling the adsorption of the dye on the oxides investigated are the nature of the oxide, the atomic distances of the surface atoms, the type of available active adsorption sites, the observed adsorption isotherms,[13] the surface potential, and the point of zero charge (PZC). It is our purpose to show how the nature of the azo dye employed, the solution pH, the degree of hydrolysis of the dye at the adsorption pH, the dye concentration, and the ionic strength of the media employed[14−16] affect the dye−oxide surface interaction. The common commercial textile azo dyes Orange II, Orange I, and Orange G on iron oxides, titania, and alumina will be systematically studied in relation to the latter parameters. Modeling of the adsorption results with their respective oxide speciations and the dye-ionized species as a function of pH was carried out to understand the electrostatic attraction between the oxides and the azo dyes.

[†] Swiss Federal Institute of Technology.

[‡] Laboratoire LEM/UMR 7569 CNRS.

(1) Zollinger, H. *Color Chemistry: Synthesis, Properties and Applications of Organic Dye and Pigments*; VCH Publishers: New York, 1987.

(2) Helz, G.; Zepp, R.; Crosby, D. *Aquatic and Surface Chemistry*; Lewis Publishing Co.: Boca Raton, FL, 1995.

(3) Ollis, F. D.; Al-Ekabi, H. *Photocatalytic Purification and Treatment of Water and Air*; Elsevier: Amsterdam, 1993.

(4) Pulgarin, C.; Kiwi, J. *Langmuir* **1995**, *11*, 519.

(5) Tincher, W. C. *Text. Chem. Color.* **1989**, *21*, 33.

(6) Morrison, C.; Bandara, J.; Kiwi, J. *J. Adv. Oxid. Technol.* **1996**, *1*, 160.

(7) Nadtochenko, V.; Kiwi, J. *J. Chem. Soc., Faraday Trans.* **1997**, *93*, 2373.

(8) Baughman, G. L.; Weber, E. J. *Environ. Sci. Technol.* **1994**, *28*, 267.

(9) Part 2 of this study: Bandara, J.; Kiwi, J.; Mielczarski, J. *Langmuir* **1999**, *15*, 7680.

(10) Stone, T. A.; Torrents, A.; Smolen, J.; Vasuderan, D.; Hadley, J. *Environ Sci. Technol.* **1993**, *27*, 895.

(11) Hug, S. J. *Colloid Interface Sci.* **1997**, *188*, 415.

(12) Hug, S.; Sulzberger, B. *Langmuir* **1994**, *10*, 3587.

(13) Vinodgopal, D.; Wynkoop, D.; Kamat, P. *Environ. Sci. Technol.* **1996**, *30*, 1660.

(14) Cunningham, J.; Sedlak, P. *J. Photochem. Photobiol. A* **1994**, *77*, 255.

(15) Cunningham, J.; Sedlak, P. *Catal. Today* **1996**, *29*, 309.

(16) Stumm, W.; Morgan, J. *Aquatic Chemistry*; Wiley: New York, 1996.

10.1021/la9900270 CCC: $18.00
Published on Web 09/16/1999

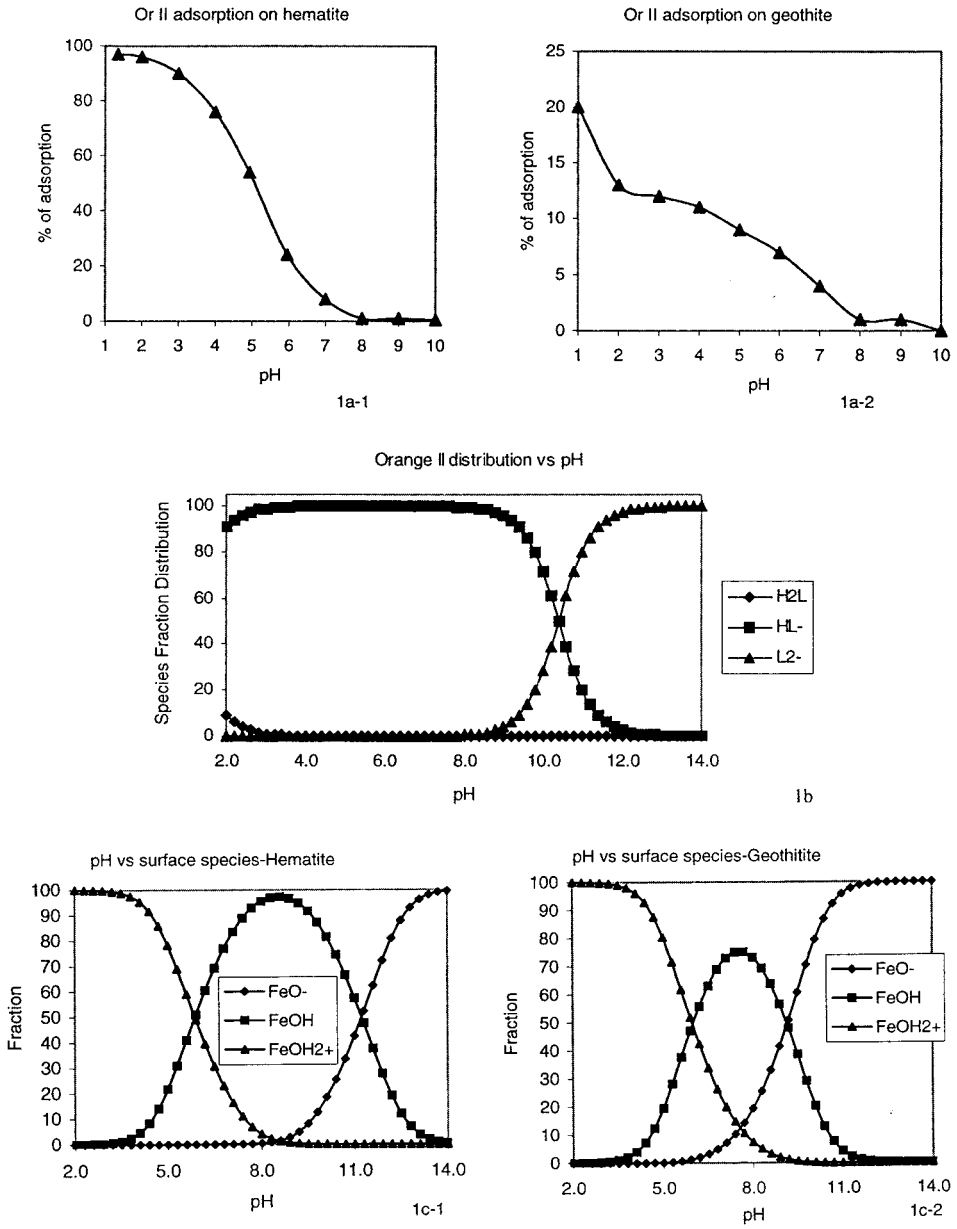

Figure 1. (a-1) Variation of the adsorption of Orange II (6×10^{-4} M) on α-Fe_2O_3 (1.5 g/L) as a function of pH. (a-2) Variation of the adsorption of Orange II (6×10^{-4} M) on α−FeOOH (1.5 g/L) as a function of pH. (b) Distribution of the Orange II species in solution as a function of pH. (c-1) Distribution of the surface species for hematite as a function of solution pH. (c-2) Distribution of the surface species for geothite as a function of solution pH.

Experimental Section

A. Materials. Orange II (Or II), Orange I (Or I), Orange G (Or G), and the acid and bases used during this work were purchased

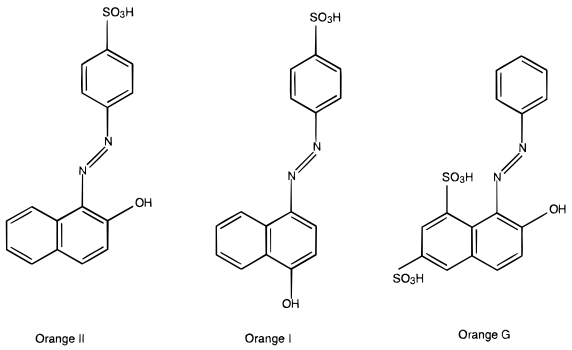

from Fluka and used as received. High-purity water was used during the experimental work ($\rho = 1$ MΩ·cm). High-surface-area α-Fe_2O_3 (150 m^2/g) was prepared according to known procedures.[17] Commercially available α-Fe_2O_3 was purchased from BASF, Ludwigshaven, Germany,[18] and had a surface area of ∼150 m^2/g. The laboratory preparation of α-FeOOH (150−160 m^2/g) used the following procedure: Fe(III) sulfate (0.15 M) was buffered at pH 6.0 with sodium acetate and hydroxylamine salt and heated at 85 °C under N_2.

The surface site density was determined from fluoride adsorption.[20,21] Fluoride adsorption experiments on oxide loadings of 2 g/L, used fluoride concentrations from 1×10^{-5} to 1×10^{-3} M. The F^- ion concentration in the supernatant solution was

(17) Cornell, R. M.; Schwertmann, U. *Colloid Polym. Sci.* **1980**, *258*, 1171.
(18) Ostertag, W. *Defazet Z.* **1979**, 434.
(19) Barret, E.; Joyner, L.; Halenda, P. *J. Am. Chem. Soc.* **1951**, *73*, 373.
(20) Gregg, S.; Sing, W. K. *Adsorption Surface and Porosity*; Academic Press: New York, 1982.
(21) Sposito, G. *The Chemistry of Soils;* Oxford University Press: New York, 1989.

determined with a Dionex ion−liquid chromatograph (ICL). The maximum amount of F^- was found by fitting the experimental data to the linearized Langmuir equation.[4,20]

The surface charge and the point of zero charge (PZC) were determined by acid−base titration of the oxide. For the titration in a 500 mL Teflon beaker, 800 mg of oxide was added to 400 mL of double-distilled water (ρ = 1 MΩ·cm). Surface charge and point of zero charge (σ) were calculated from the acid−base titration

$$\sigma = F(\Gamma_{H^+} - \Gamma_{OH^-}) \quad (1)$$

where Γ_{H^+} and Γ_{OH^-} are the adsorption densities of H^+ and OH^- in moles per square meter and F is the Faraday constant.

B. Adsorption Isotherms. The extent of the adsorption was calculated as follows

$$n_2^s = \frac{\Delta C V}{W} \quad (2)$$

where n_2^s is the adsorbed amount (mol/g), ΔC = initial concentration − final concentration, V is the volume, and W is the weight of the oxide. The concentration of azo dye in the supernatant was determined by HPLC or spectrophotometrically and subtracted from the initial concentration to determine the adsorbed amount in each case.

C. FTIR. Infrared diffuse reflectance infrared fourier transform (DRIFT) spectra of the adsorbed species, azo dyes, and their degradation products on iron titanium and aluminum oxides were recorded on a Bruker IFS 55 FTIR spectrophotometer equipped with an MCT detector and a reflection attachment. The diffuse reflectance accessory was from Harrick Co. The oxide samples after adsorption from solution were filtered, dried in air, and diluted in KBr at a 1:5 ratio. Some of the samples were heated to a temperature of 120 °C to remove physisorbed water.

D. X-ray Diffraction and N_2 Surface Area Measurements. The crystalline structure was determined using the X-ray powder diffraction method with a Regaiku III/B MAX diffractometer using Ni-filtered Cu Kα radiation. X-ray diffraction analysis revealed that both commercially available oxides and lab-prepared α-Fe_2O_3 and α-FeOOH are 100% crystalline. Other commercial oxides (TiO_2 anatase and rutile, α-Al_2O_3, and α-AlOOH) were also found to be 100% crystalline.

Specific surface areas were determined with a BET Carlo Erba Sorptomatic-1900 unit, and the N_2 desorption isotherm was calculated using the cylindrical pore model of Barret, Joyner, and Halenda.[19] Anatase (100%) and rutile (100%) were from British Tioxide, and both samples had the same surface area (50 m^2/g). γ-Al_2O_3 and α-Al_2O_3 were Engelhard and Reactor Lab reagents and used as received. BET N_2 adsorption measurements showed that the anatase and rutile forms had a surface area close to 50 m^2/g, while γ-Al_2O_3 with 170 m^2/g and α-Al_2O_3 with 16 m^2/g had very different surface areas. The laboratory-prepared and commercial α-Fe_2O_3 showed about the same surface area (150−160 m^2/g), as had the laboratory-prepared α-FeOOH, with a surface area around 150 m^2/g.

For the adsorption experiments, either laboratory-prepared or commercial α-Fe_2O_3 was used throughout this work.

E. Modeling. The Acuchem program written by W. Braun, J. T. Herron, and D. Kahaner (National Bureau of Standards, Gaithersburg, MD 20899) was used for modeling the reaction sequence on the basis of the experimental data found during this study. The fitting was carried out with the program MatLab 4.2 written by B. Volker and S. Hug of EAWAG (Zürich) in conjunction with Acuchem software. In this way the simultaneous differential equations corresponding to the reaction scheme were solved during this study.

The ionization of Orange II as a function of pH was calculated using the two known pK_a values of this dye and eqs 3 and 4 in order to compute at each pH value the ionized fraction via the ChemEQL program (version 2.0). Orange II (Figure 1a) adsorbs on Fe oxides under acid and neutral conditions. The behavior of the amphoteric oxide in solution was seen to be a function of the pH of the solution due to the interaction of the oxide surface with the H^+. The purpose of all surface models by ChemEQL is to consider electrostatic interactions between surface and sorbing ions. The generalized two-layer model (diffuse/GTL) has been chosen to account for the electrostatic interaction between charges and takes into account the specific surface area, the concentration of the surface sites, and the ionic strength of the solution.

For each of the eqs 7−10 (see text, next section) the model used is applied with a fitting test parameter for the adsorption coefficient. The good agreement found for the pH dependency of the adsorption is taken as a proof of the validity of the model employed.

Results and Discussion

A. Modeling of the Adsorption of Orange II on Iron Oxides. Shift in the ζ Potentials. Figure 1a presents the adsorption of Orange II on α-Fe_2O_3 and α-FeOOH at different pH values to observe the effect of pH on the adsorption of the dye. The adsorbed amounts are given as the percentage weight of dye per gram of oxide. Adsorption was carried out either from acidic pH to basic or vice versa for a solution of Orange II (0.60 mM) and 1.5 g/L of α-Fe_2O_3 or α-FeOOH with the same surface area. The equilibrium was attained within 1−2 min for both iron oxides at a pH convenient for high Orange II adsorption (see Figure 1). A 5-fold higher adsorption was observed with α-Fe_2O_3 than in the case of α-FeOOH. The adsorption of Orange II was seen to increase toward more acid pH values (Figure 1a). As the pH moves to pH values > 7.0, the adsorption is seen to be negligible for both iron oxides under consideration.

To understand the interaction of the adsorbate and the adsorbent, the speciation of both species in solution as a function of pH was followed, and the results are shown in Figure 1b and c. Figure 1b shows the acid ionization of Orange II as a function of solution pH. The calculation of the distribution species of Orange II in solution is based on the pK_{a1} values at 11.4 for the deprotonation of the naphthalene OH, as found by titration (see Experimental Section). The literature value pK_{a2} ∼ 1 for the deprotonation of the SO_3H group is taken as the second pK value of Orange II.[1,13]

According to the species distribution of Orange II in Figure 1b above pH 12, only the negative L^{2-} or OR^{2-} exists in solution. Between pH values 8 and 12, HL^- or HOR coexists in solution with L^{2-}. Below pH 8 most of the Orange II exists as HL^- or H_2OR. The distribution of ionic species as a function of pH was calculated from their pK_a values (see below, eqs 3 and 4) in Figure 1c. The ionic strength of the solution used was 0.1 M, which is usually employed for adsorption studies.[9−12]

The fraction of >FeOH decreased to negligible levels at pH 3.0 for both oxides. Figure 1c shows that the $>FeOH_2^+$ fraction increases as the pH becomes more acidic. The fractions of $>FeOH_2^+$ on the α-Fe_2O_3 surface are seen in Figure 1c-1 to be 50% at pH 6.0, 70% at pH 5.0, and 90% at pH 4.0. Similar behavior was observed for α-FeOOH in Figure 1c-2. The fraction of >FeOH was observed to attain negligible levels at pH 3.0 for both iron oxide surfaces.

No adsorption of L^{2-} takes place on hematite and geothite, as indicated in Figures 1b and c. Adsorption of Orange II takes place only at pH < 7, where L^{2-} is practically not present in solution. Above pH 7 no adsorption is observed, since the adsorbent and adsorbate exist in their negative forms: L^{2-} and $>FeO^-$. Orange II adsorption on α-Fe_2O_3 and α-FeOOH begins to appear around pH 7 and increases to pH 3.5, where it levels off. Therefore, the adsorption shown in Figure 1a-1 and 1a-2 is readily accounted for by the electrostatic interaction of the species HL^- and $FeOH_2^+$, leading the adsorption shown in Figure 1a.

Table 1. Parameters of the Oxides Used to Model Surface Speciation

oxide	B.E.T. (m^2/g)	$10^6 F_{max}$ (mol/m^2)	no. of sites ($sites/nm^2$)	$-\log K_{a1}^{s}$ [a]	$-\log K_{a2}^{s}$ [b]	pH_{PZC}
α-Fe_2O_3	150−160	9.81	5.91	6.70	10.4	8.4−8.5
α-FeOOH	150−160	8.30	5.00	6.78	8.35	7.55
TiO_2(anatase)	55	5.32	3.21	5.4	7.6	6.50
TiO_2(rutile)	50	6.15	3.71	4.8	7.4	6.13
γ-Al_2O_3	170	2.25	1.35	7.5	10.0	8.75
α-Al_2O_3	16	1.50	0.90	8.1	10.8	9.10[c]

[a] Acidity constant K_{a1}. [b] Acidity constant K_{a2}. [c] Reported value was taken.

The chemical reactions and the corresponding mass action expression required by the diffuse-layer model are shown below by eqs 3−10.[16,20] Equations 3−6 represent the equilibria among species due to surface protonation as a function of pH during the acid−base titration. Experimental adsorption data fitting was carried out for the four different types of absorption stoichiometries in eqs 7−10. Equations 7−10 represent the possible surface complexes formed during the adsorption of the dye on the iron oxide surface with the species distribution found for Orange II and α-Fe_2O_3 in eqs 3−6 below

$$H_2L \leftrightarrow HL^- + H^+ \qquad K_{a1} = \frac{[HL^-][H^+]}{[H_2L]} \tag{3}$$

$$HL^- \leftrightarrow L^{2-} + H^+ \qquad K_{a2} = \frac{[L^{2-}][H^+]}{[HL^-]} \tag{4}$$

$$>FeOH_2^+ \leftrightarrow >FeOH + H^+ \qquad K_{a1} = \frac{[>FeOH][H^+]}{[>FeOH_2^+]} \tag{5}$$

$$>FeOH_2^+ \leftrightarrow >FeO^- + H^+ \qquad K_{a2} = \frac{[>FeOH^-][H^+]}{[>FeOH]} \tag{6}$$

$$>FeOH + L^{2-} \leftrightarrow >FeL^- + HO^- \qquad K_{a1} = \frac{[>FeL^-][OH^-]}{[>FeOH][L^{2-}]} \tag{7}$$

$$>FeOH + HL^- \leftrightarrow >FeHL + HO^- \qquad K_{a2} = \frac{[>FeL^-]}{[>FeOH][HL^-]} \tag{8}$$

$$>FeOH_2^+ + H_2L \leftrightarrow >FeHL + H_2O + H^+ \qquad K_{a3} = \frac{[>FeHL][H^+]}{[>FeOH_2^+][H_2L^-]} \tag{9}$$

$$>FeOH_2^+ + HL^- \leftrightarrow >FeL^- + H_2O + H^+ \qquad K_{a4} = \frac{[>FeHL^-][H^+]}{[>FeOH_2^+][HL^-]} \tag{10}$$

In eq 6 a neutral unoccupied surface site is noted by >FeOH. Equation 7 shows a surface reaction where only one position of the oxide surface is available. In this case the adsorption of one ligand involves the reaction of one H^+ during the conversion of OH^- into H_2O. The latter step opens a vacancy in the inner coordination sphere of the oxide surface that can be occupied by an incoming ligand.[16] It is seen that, for the adsorption of Orange II on both iron oxides, the double-layer model is able to represent the experimental data obtained in Figure 1. As a consequence, reactions 7 and 8 occurring at pH > 7 cannot contribute to the observed adsorption. The evidence presented suggests that the adsorption could be attributed to reaction 10 due to the electrostatic attraction between HL^- and $FeOH_2^+$. Reaction 10 provides the best fit when the pH dependency of the Orange II adsorption was examined and modeled through reactions 7−10, as described in the Experimental Section, confirming the reaction mechanism suggested above.

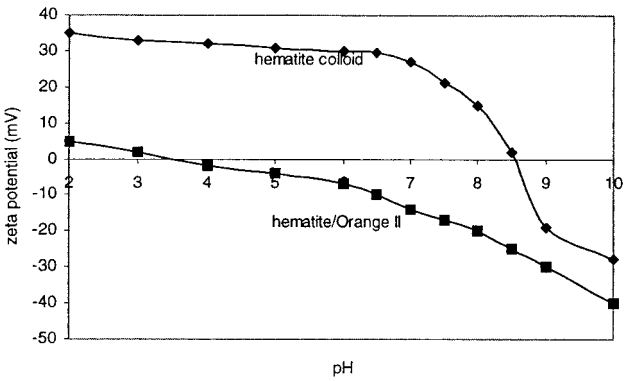

Figure 2. Zeta potential of (a) α-Fe_2O_3 and (b) α−FeOOH particles as a function of solution pH in a solution with ionic strength 0.1 M.

Figure 1a-1 shows that α-FeOOH presents poorer adsorption properties toward Orange II than α-Fe_2O_3. The Orange II adsorption on α-FeOOH in Figure 1a-2 is approximately one-fifth of the one observed with α-Fe_2O_3. Similar poor adsorption properties of α-FeOOH have been reported toward oxalates[25] and citrates.[26] This is surprising, since the surface area and the density of surface states for α−Fe_2O_3 and α−FeOOH are about the same, as seen in Table 1. This is associated with structural differences inherent to the surfaces of α-Fe_2O_3 and α-FeOOH. This point will be discussed below in section G.

The ζ potentials of hematite colloids and in the presence of Orange II are shown in Figure 2. It is observed that the adsorption of the azo dyes shifts the PZC of the hematite. The values of the ζ potentials in Figure 2 are calculated from the electrophoretic mobilities.[16] The latter values are shown to shift to more negative values in the presence of Orange II due to the adsorption of Orange II on the iron colloid. Kally and Matijevic[27] also observed a similar shift of adsorption when oxalate is adsorbed on iron oxides. The colloidal particles loaded with Orange II exhibited a negative electrophoretic mobility in the case of hematite above pH 8.5 and in the case of hematite with Orange II adsorbed on the surface above pH 3.5, as shown in Figure 2. The equilibria show the existence of the negatively charged surface species as $>FeOHL^-$, $>FeOL^-$, and

(22) Bates, R. G. *Determination of pH, Theory and Practice*; John Wiley: New York, 1973.
(23) Kallay, N.; Matijevic, E. *Langmuir* **1985**, *195*, 1.
(24) Cornell, R. M.; Schindler, P. W. *Colloid Polym. Sci.* **1980**, *258*, 1171.
(25) Hsu, W.; Yu, R.; Matijevic, E. *Dyes Pigments* **1992**, *19*, 179.
(26) Giesche, H.; Matijevic, E. *Dyes Pigments* **1991**, *17*, 323.
(27) Zhang, Y.; Kally, N.; Matijevic, E. *Langmuir* **1985**, *201*, 1.

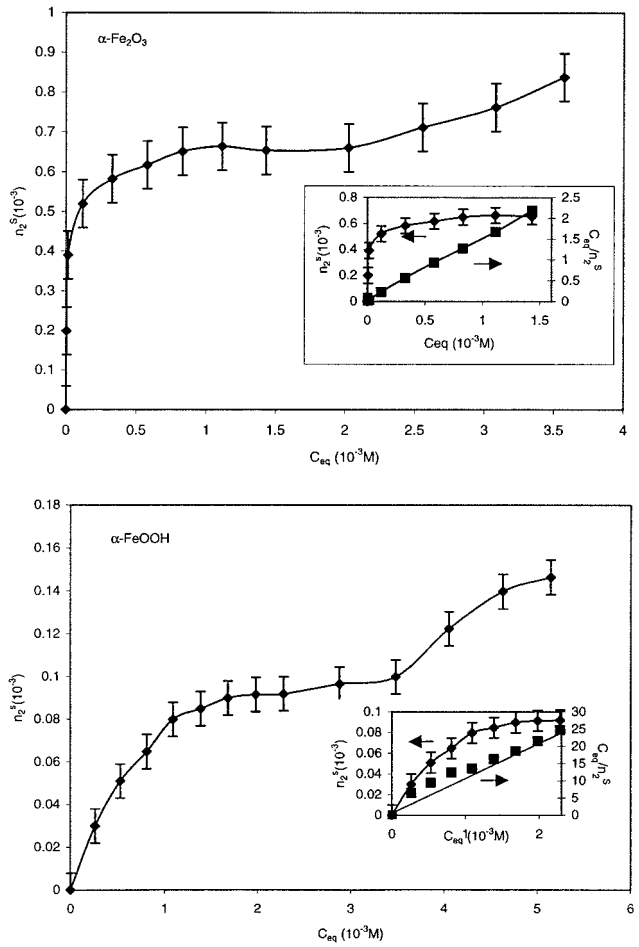

Figure 3. (1) Adsorption isotherm of Orange II at pH 3.5 for α-Fe_2O_3. (2) Adsorption isotherm of Orange II at pH 3.5 for α-FeOOH.

>FeL^-. The species >$FeOL^-$ are seen in eqs 8 and 10. This indicates that >$FeOL^-$ particles are present in solution up to pH ∼ 4 and fully protonate at more acidic pHs.

B. Adsorption Isotherms of Orange II on α-Fe_2O_3 and α-FeOOH. The adsorption isotherms for Orange II are shown in Figure 3 for α-Fe_2O_3 and α-FeOOH. The adsorption of Orange II increases toward a plateau in both cases as the concentration of the dye is increased. A slow increase after the plateau concentration region suggests multilayer adsorption increasing at higher dye concentrations.[14,15] In Figure 3 n_2^s is the number of dye molecules adsorbed per gram of oxide. The behavior of n_2^s is usually stated as a function of the dye equilibrium concentration C_{eq}

$$n_2^s = \frac{(n^s K C_{eq})}{(1 + K C_{eq})} \tag{11}$$

where n^s is the number of adsorption sites and K is the equilibrium constant for dye adsorption. At low equilibrium concentrations $KC_{eq} \ll 1$, and the plot of n_2^s versus C_{eq} is linear with a slope $n^s K$. In this low-concentration region the expected linearity is seen in the insets in Figure 3a and b up to an equilibrium concentration of 2×10^{-3} M. However, Cunningham and Srijaranai[30] argued that due to competition for the available sites with solvent molecules it is unrealistic to expect that all the available sites on the oxide surface could be occupied by dye molecules. In this case the adsorption data should be linearized by

$$\frac{C_{eq}}{n_2^s} = \frac{1}{K n_2^s(\max)} + \frac{C_{eq}}{n_2^s(\max)} \tag{12}$$

$$\frac{C_{eq}}{n_2^s} = \frac{N_A \sigma^\circ}{A_{sp} K} + \frac{N_A \sigma^\circ}{A_{sp}} \tag{13}$$

where $n_2^s(\max)$ represents the limiting number of dye molecules that can be adsorbed onto a gram of oxide, σ° is the average area that each dye molecule occupies on the surface monolayer, A_{sp} is the adsorbent surface area, and N_A is Avogadro's number. The plots of C_{eq}/n_2^s versus C_{eq} for Orange II with α-Fe_2O_3 and α-FeOOH are shown in the insets of Figure 3a and b, respectively. The value of 6.58×10^{-4} for n_2^s represents the maximum moles of Orange II that can be adsorbed for a monolayer on a gram of oxide. A value of 4.35×10^5 L/mol was determined for the equilibrium constant K for α-Fe_2O_3. Assuming a specific surface area of 150 m^2/g for α-Fe_2O_3, σ° could be calculated for the Orange II molecules on α-Fe_2O_3. The calculated area for a molecule of Orange on α-Fe_2O_3 was 0.40 nm^2. The values for n_2^s, K, and σ° calculated from the adsorption isotherm of Orange II on different oxides are found in Table 2.

Table 2. Adsorption Sites (n_2^s), Equilibrium Constants of Orange II Adsorption (K), and Surface Area (σ°) on Different Oxides

oxide	$10^{-4} n_2^S(\max)$	K	σ° (nm^2)
α-Fe_2O_3	6.58	4.35×10^5	0.40
α-FeOOH	0.98	1.29×10^3	0.44
TiO_2(anatase)	1.94	4.37×10^3	0.42
TiO_2(rutile)	2.03	5.46×10^3	0.40
γ-Al_2O_3	8.81	2.60×10^4	0.38
α-Al_2O_3	1.17	5.01×10^3	0.32

Table 3. Adsorption Sites (n_2^s), Equilibrium Constants of Dye Adsorption (K), and Surface Area (σ°) on Hematite

dye	$10^{-4} n_2^S(\max)$	K	σ° (nm^2)
Orange II	6.58	4.35×10^5	0.40
Orange I	5.51	4.11×10^5	0.46
Orange G	2.48	2.19×10^4	1.00

The adsorptions of other azo dyes were assessed on iron oxides to see how the dye structure affects the extent of adsorption (see Experimental Section). Orange G presented the lowest equilibrium constant K on α-Fe_2O_3. Orange I shows similar values of n_2^s and K to those for Orange II in Table 3.

The lower K values observed for Orange G in Table 3 are due to two bulky SO_3H^- groups in the naphthalene ring which prevent Orange G from approaching closely the iron oxide surface. It is also possible that both sulfonic groups participate in the adsorption, and therefore, a larger number of >Fe−OH sites are blocked by Orange G molecules than in the case of monodentate single sulfonic complex formation occurring with Orange I or Orange II. The average area per molecule of Orange G was higher than those of Orange II and Orange I, which confirms the preceding argument. Similar to Orange II, Orange I and Orange G dyes were also observed to adsorb poorly on α-FeOOH.

(28) Halmann, M. *Photodegradation of Water Pollutants*; CRC Press: Boca Raton, FL, 1996.
(29) Hansen, R. S.; Craig R. P. *J. Phys. Chem.* **1954**, *58*, 212.
(30) Cunningham, J.; Srijaranai, S. J. *Photochem. Photobiol. A: Chem.* **1991**, *58*, 361.

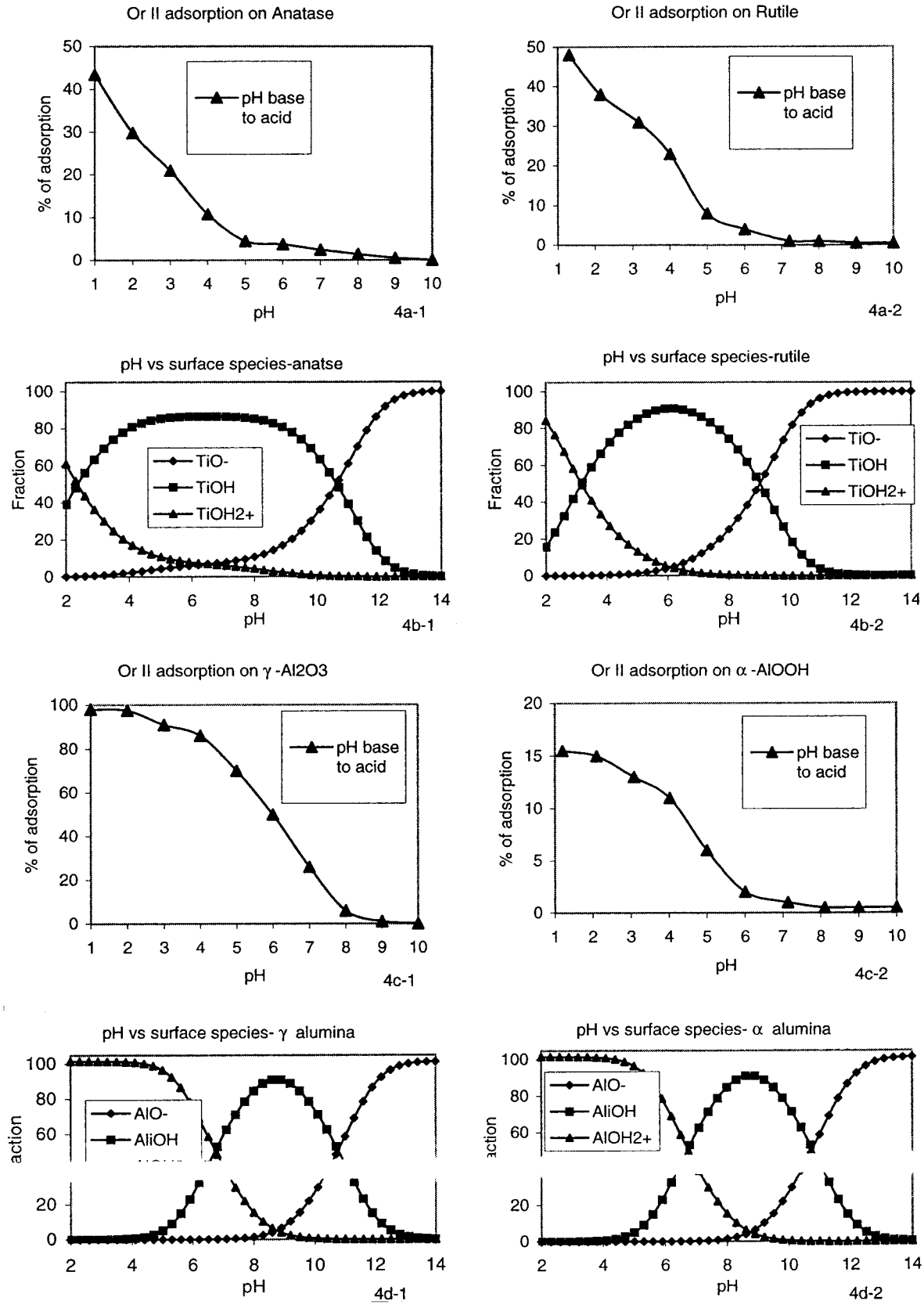

Figure 4. (a-1) Variation of Orange II (6×10^{-4} M) adsorption on anatase (1.5 g/L) as a function of pH. (a-1) Distribution of the surface species for rutile as a function of solution pH. (b-1) Distribution of the surface species for anatase as a function of solution pH. (b-2) Distribution of the surface species for rutile as a function of solution pH. (c-1) Variation of the adsorption of Orange II (6×10^{-4} M) on γ-Al_2O_3 (1.5 g/L) as a function of pH. (c-2) Variation of the adsorption of Orange II (6×10^{-4} M) on α-Al_2O_3 (1.5 g/L) as a function of pH. (d-1) Distribution of the surface species for γ-Al_2O_3 as a function of solution pH. (d-2) Distribution of the surface species for α-Al_2O_3 as a function of solution pH.

C. Adsorption of Orange II on Ti and Al Oxides. The adsorption of Orange II was also carried out on TiO_2 (anatase and rutile), as shown in Figure 4a, and on γ-Al_2O_3 and $\alpha-Al_2O_3$, as seen in Figure 4c. From Figure 4b it can be seen that the adsorption begins to be meaningful as the amount of $TiOH_2^+$ increases for both anatase and rutile, resembling the increase in the fraction of $TiOH_2^+$ (Figure 4b). With anatase and rutile the adsorption is seen to be below 100% for Orange II (Figure 4a). However, with anatase the Orange II adsorption extended beyond pH 7. This was not the case with rutile. The presence of a small amount of $TiOH_2^+$ beyond pH 7 was observed with anatase but not with rutile in Figure 4b-1. It seems, therefore, that $TiOH_2^+$ is responsible for the dye adsorption on titania surfaces, suggesting that electrostatic attraction leads to the observed adsorption. The latter process would involve the adsorption of HOR^- on titania in a similar way to that for the case of α-Fe_2O_3. Similar results were obtained with α-Al_2O_3 and γ-Al_2O_3, as reported in Figure 4c-1 and c-2. Also in this case, the $AlOH_2^+$ seems to be the species involved in the adsorption of the dye on the alumina surfaces (Figure 4d-1 and d-2). γ-Al_2O_3 shows a much higher adsorption of Orange II. The n_2^s, K, and σ° values calculated from the adsorption isotherm for anatase and rutile, α-Al_2O_3, and γ-Al_2O_3 are shown in Table 2.

D. Effect of Inorganic and Organic Anions on Adsorption of Orange II on α-Fe_2O_3 and α-FeOOH. Counteranions in solutions of Orange II were observed to compete for the available binding sites on the oxides used as adsorbing substrates. The NO_3^- and SO_4^{2-} ions adsorbed up to 1.2×10^{-4} mol of nitrates and 1.5×10^{-4} mol of sulfates per gram of α-Fe_2O_3 at pH values between 3 and 4.0. The amount of chloride adsorption was found to be low, about six times lower. When Orange II was adsorbed from solution in the presence of Cl^- and NO_3^-, the amount adsorbed was not affected by the presence of the latter anions in solution. However, the adsorption of Orange II on α-Fe_2O_3 decreased dramatically when SO_4^{2-} and SO_3^{2-} were also added in solution along with the azo dye, indicating the competitive nature of these anions with the dye during the adsorption process, suggesting that the sulfonic group of Orange II is the binding site for this dye on α-Fe_2O_3 and α-FeOOH. This point will be taken up in the FTIR section (E) below. Salicylic acid with COOH and OH groups added to the Orange II solution did not practically hinder the adsorption of the dye on the oxide. A decrease of $<4\%$ was observed, indicating that salicylic acid, having no sulfonic groups, is not competitive during the adsorption of Orange II on iron oxides.

E. Adsorption Mechanism of Azo Dyes on Oxide Surfaces. FTIR Studies. The observation that no dye adsorption takes place in the presence of sulfate or sulfite confirms the participation of the sulfonic group of Orange II during adsorption into the iron surface This bond formation could occur by (a) chelating bidentate, (b) bridged bidentate, or (c) unidentate complex formation with the metal through an oxygen.

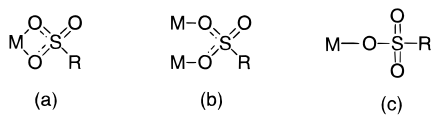

Figure 5 shows the FTIR adsorption results for Orange II in solution and on α-Fe_2O_3 and α-FeOOH, respectively. Due to symmetry considerations the —N=N— stretching mode of the symmetrically substituted trans-isomer is usually IR forbidden. The —N=N— shows a weak stretching band when the trans azo compound is asymmetrically

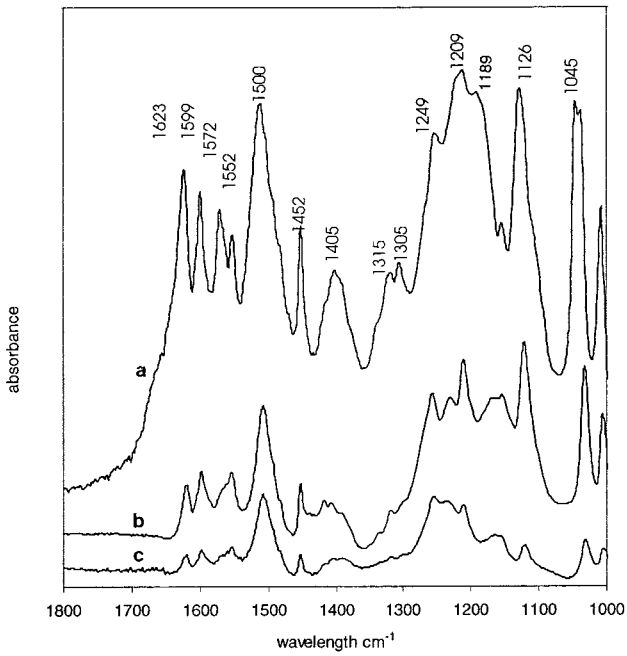

Figure 5. FTIR spectra for (a) Orange II in aqueous solution, (b) Orange II adsorbed on α-Fe_2O_3, and (c) Orange II adsorbed on α-FeOOH. IR transmission mode employed in all cases.

substituted. Free Orange II in solution has asymmetrically substituted —N=N— bonds with a weak stretching band around 1450−1500 cm^{-1}. The weak peak at 1452 cm^{-1} present at the shoulder of the OH bending peak is assigned to the —N=N— bond. Kamat[13] assigned the 1500 cm^{-1} band to —N=N— bond vibrations or to aromatic ring (C=C) vibrations sensitive to the interaction with azo bonds. The band at 1500 cm^{-1} is too strong to be ascribed to a trans azo bond, and the peak seems to correspond to C=C stretching vibrations. Also the bands at 1552, 1572, 1599, 1623, and 1452 cm^{-1} were assigned to C=C stretching vibrations.[32] The CH bands were clearly seen at 832 and 750 cm^{-1}. The weak peaks at 1405 and 1318 cm^{-1} were due to the bending OH deformation while the band at 1256 cm^{-1} was assigned to the COH stretching vibration. The SO_2 symmetric and asymmetric vibrations were seen at 1190 and 1305 cm^{-1}, respectively.[31,32] The peaks of adsorbed Orange II on α-Fe_2O_3 and α-FeOOH were similar to those of Orange II except for the peaks of the sulfonic groups. The symmetric peak at 1190 cm^{-1} and the asymmetric peak at 1305 cm^{-1} for vibrations of the —O—S—(O_2) group almost disappeared or were very weak after adsorption. This suggests the participation of single and double sulfur links S—O and S=O in the bond formation with the oxide surface, precluding formation of an unidentate complex.

F. Modeling Orange II Adsorption on Iron Oxides by Semiempirical Methods. Semiempirical methods[34] and ab initio methods[35] have been used to optimize the adsorbed molecule. The optimized geometrical structure of Orange II with the lowest molecular energy was used during the modeling of the adsorption on α-Fe_2O_3. For

(31) Centi, G., Ed. *Environmental Catalysis*; Ital. Chem. Soc. Pub. Rome, 1995.
(32) Silverstein, R.; Clayton, T.; Morril, T. *Spectrophotometric Identification of Organic Compounds*; Wiley: New York, 1991.
(33) Lin Vien, D.; Norman, C.; Grasselli, J. *Handbook of Infrared and Raman Characteristic Frequencies of Organic Molecules*; Academic Press: New York, 1991.
(34) Nakatsuji, H.; Fukunishi, Y. *Int. J. Quantum Chem*. **1992**, *42*, 1101.
(35) Sauer, J. *J. Phys. Chem*. **1987**, *91*, 2315.

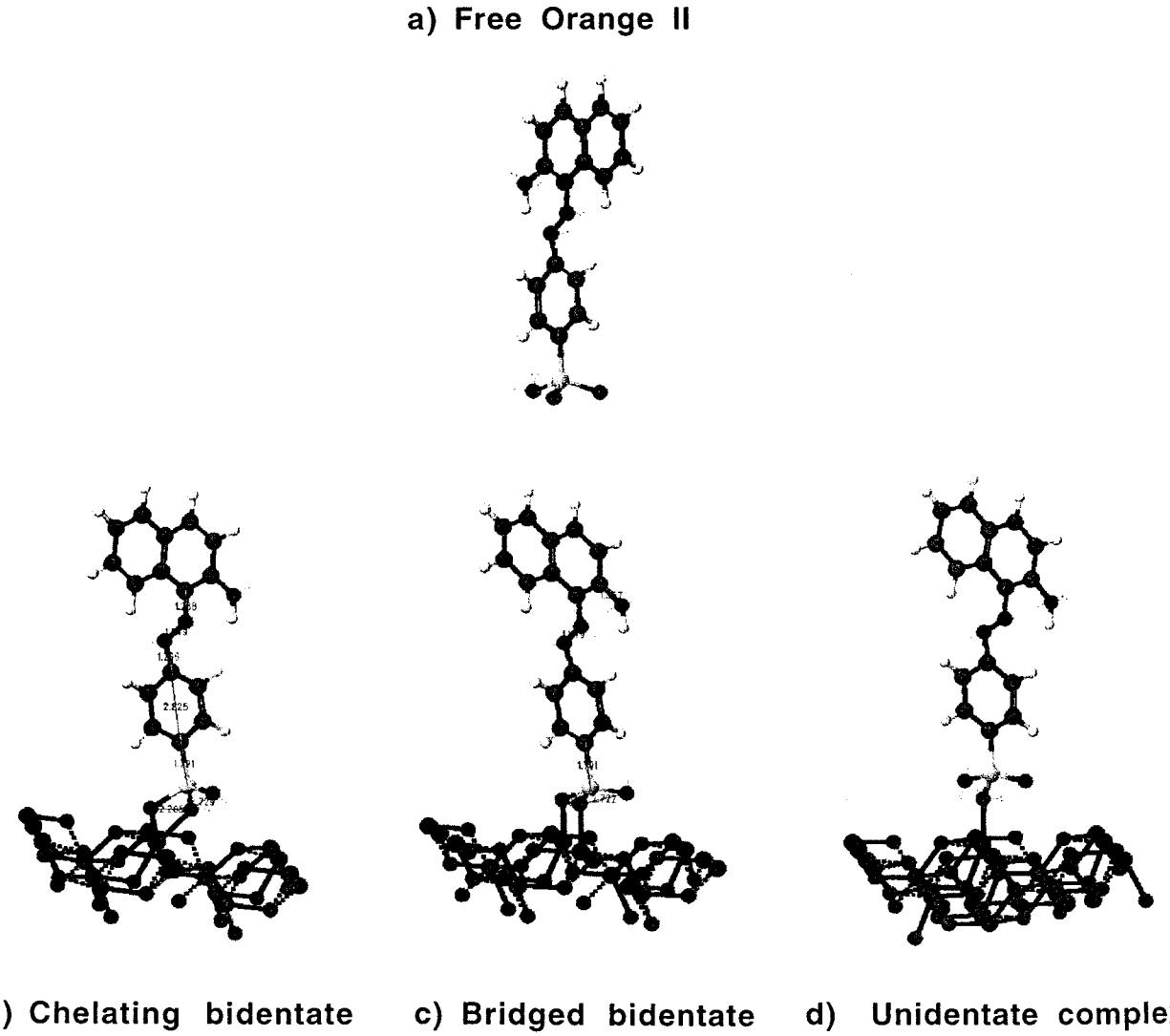

Figure 6. Semiempirical structures of (a) Orange II adsorbed on the α-Fe_2O_3 (100) crystalline plane, (b) the chelating bidentate complex, (c) the bridged bidentate complex, and (d) the unidentate complex.

semiempirical calculations, the CAChe Mechanics program[36] was employed. The crystal lattice was calculated from the unit cell parameters and the fractional coordinates found for the unit cell. The [100] crystalline face of α-Fe_2O_3 was selected, since it is the dominant crystalline face of this iron oxide. In this calculation, the cluster geometry is fixed in the crystal lattice position. However, the CAChe program precludes the consideration of surface changes taking place during adsorption. Therefore, these changes could not be taken into account in these calculations. Only the geometry of the adsorbate was optimized using the energy gradient method. Optimization was carried out for the possible structures a−c discussed above, and the results are shown in Figure 6. Orange II, which was used to model the adsorption, is shown in Figure 6a. The optimized geometry of the adsorbed Orange II on hematite is shown in Figure 6b,c and d, corresponding to the structures a, b, and c, respectively, above in section E.

The Fe−Fe atomic distances in α-Fe_2O_3 are as follows: for the face shared arrangement, 2.89 Å; for the edge-shared octahedra, 2.97 Å; and for a corner-shared octahedra, 3.39 Å. The sulfonic group of Orange II has atomic distances and bond angles as follows: The atomic distances between two O atoms for S−(OH) and for S═O are 2.67−2.68 Å. The angles between S−(OH) and two S═O groups are 35.32° and 38.19°. The S−O and S═O bond lengths are 1.75 and 1.537 Å, respectively. The fact that the matching of the Fe−Fe atomic distance with the bond distance (O−O) in the sulfonic groups (−O−S−(O−O)) makes configuration b, and not a or c in section E, the configuration of choice is due to the interatomic distance required for the adsorption of Orange II on hematite. The metal−oxygen bond length is considered as a measure of the strength of the surface complex, while the O−S−(O−O) angles can be considered as a measure of the stability of the complex.[34] For structure b, the Fe−O distance is shorter than that in a, suggesting a chelate bidentate with a more stable complex than the bridged bidentate complex. The angles in the bridged structure decrease to achieve a better orbital overlap, since in this case two O atoms share their orbitals with the Fe atom. In the chelate structure a the O atom interacts only with one Fe atom, generating strain on the −O−S−(O−O) angles which cause the bridged bidentate complex to be unstable. With regard to the possibility of the formation of c) in the case of the unidentate complex, FTIR shows that when Orange II is adsorbed on iron oxide, both the symmetric and

(36) Cornell, R. M.; Schwertmann, U. *The Iron Oxides, Structures, Properties, Reactions, Occurrence and Uses;* VCH Publishers: Weinheim, Germany, 1996.

Table 4. Calculated Bond Angles and Distances for Sulfonic Groups Used in the Calculations of Figure 6

	structure a	structure b	structure c	free or II
S—(OH) and S═O distances	2.205 Å	2.946 Å	2.714 Å	2.678 Å
	2.729 Å	2.723 Å	2.697 Å	2.681 Å
S—(OH) and S═O angle	30.195	33.08	33.35	35.32
S—(OH) distance	1.73 Å	1.759 Å	1.752 Å	1.75 Å
S—O—Fe distance	1.93 Å	1.91 Å	1.91 Å	

asymmetric vibrations of the sulfonic group change. The structure b suggested by FTIR was confirmed by modeling of the adsorption. The bond angles and distances in Figure 6 have been calculated and are shown in Table 4.[34,35]

Figure 1a-2 presents the adsorption of azo dye on α-FeOOH as being lower than that on α-Fe_2O_3. Both oxides have the same surface area and OH sites/nm^2 (Table 1). The absorption properties of both iron oxides could not be correlated to the numerical values of the oxide surface area or the number of available OH surface sites.

The dominant crystalline face of α-FeOOH is known to be [110].[36] The Fe—Fe lattice distances are 3.01 and 3.28 Å for the edge-shared octahedra and 3.46 Å for the corner-shared octahedra, respectively. The Fe—Fe lattice distance is higher in α-FeOOH than in the case of α-Fe_2O_3. Therefore, the sulfonic group O—S—(O—O) with a lattice distance 2.68 Å would interact preferably with α-Fe_2O_3 than with α-FeOOH, as shown below.

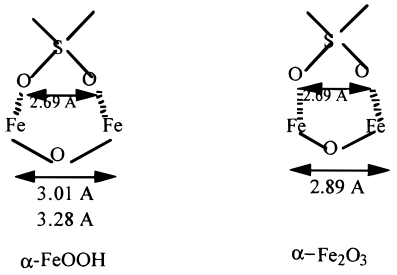

G. FTIR Studies of the Adsorption of Orange I and Orange G on Iron Oxides. For comparison, adsorption of different azo dyes with different functional groups (see Experimental Section) was carried out on α-Fe_2O_3 and α-FeOOH and the results are shown in Figure 5b. This figure shows the FTIR spectra of Orange I and Orange G adsorbed on α-Fe_2O_3. The IR patterns of free Orange I and Orange G are almost similar to the IR pattern of Orange II. In both spectra, bands at 1550—1660 and 1452 cm^{-1} were assigned to C═C stretching vibrations. The CH bands are seen around 830 and 750 cm^{-1}. The band at 1256 cm^{-1} was assigned to the C—O—H stretching vibration. The —O—S—(O—O)— symmetric and asymmetric vibrations are located at 1190 and 1319 cm^{-1}, respectively.[35,36] The —N═N— bond in Orange G could not be identified. This may be due to a weak azo bond overlapping with strong C═C vibrations. But for Orange I, a weak peak appeared at 1450 cm^{-1} for the azo bond vibration. For Orange I and Orange G molecules adsorbed on iron oxides, the observed peaks were similar to those for free Orange I and Orange G in solution except for the peaks of the sulfonic group. The symmetric (1190 cm^{-1}) and asymmetric (1305 cm^{-1}) vibrations in the case of the last two Orange dyes in solution assigned to O—(SO_2)— disappeared or were weak. This suggests the participation of both S═O and S—O groups in bond formation with the oxide surface, similar to Orange II adsorption on α-Fe_2O_3.[37] This is indicative that the azo dye adsorption mechanism on iron oxides is the same for the three different azo dyes used in this work.

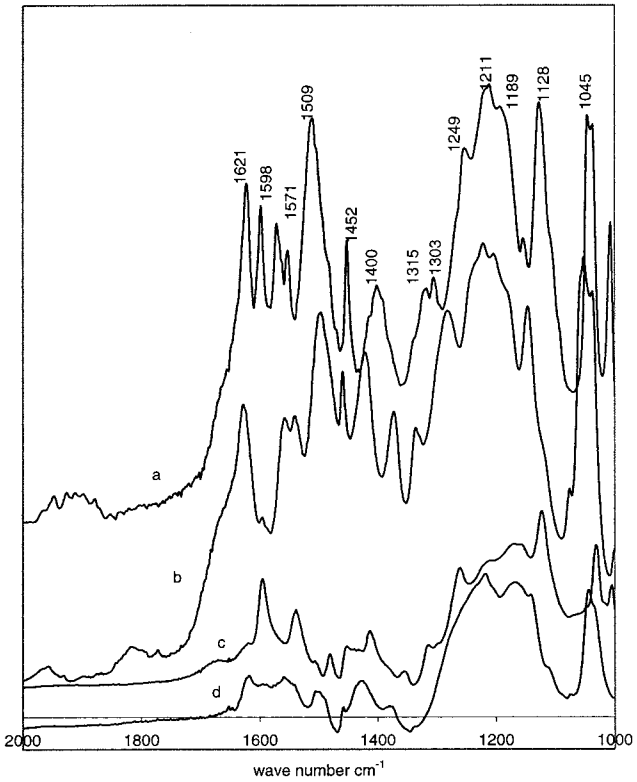

Figure 7. FTIR spectra for adsorbed Orange II on (a) anatase, (b) rutile, (c) α-Al_2O_3, and (d) γ-Al_2O_3.

H. Comparison of the Orange II Adsorption Mechanisms on TiO_2 and γ-Al_2O_3. Figure 7 shows the adsorption of Orange II on Ti and Al oxides. The IR patterns of the adsorbed dye on alumina and titanium oxides are seen to be similar. For both oxides, the symmetric vibration of O—S—(O_2) of the three azo dyes observed at 1190 cm^{-1} was replaced by a broad band at 1150 cm^{-1}. The asymmetric vibration O—S—(O_2) at 1318 cm^{-1} was observed to decrease drastically on the Ti and Al oxides. The latter observation is similar to that for Orange II being adsorbed on α-Fe_2O_3. This suggests a common adsorption mechanism taking place for the three oxides under study. The amount of azo dye adsorption on TiO_2, either anatase or rutile, was substantially lower than that on α-Fe_2O_3. This is due to a higher Ti—Ti atomic distance in the TiO_2 lattice structure. The Ti—Ti atomic distances are 3.79 and 3.57 Å, respectively, for anatase and rutile. These distances are much higher than the Fe—Fe atomic distance (2.89 Å) in α-Fe_2O_3 and are not compatible with the O—S—(O_2) distance in the sulfonic group of 2.69 Å, as mentioned before. Therefore, the SO_3^- group interacts more favorably with α-Fe_2O_3 than TiO_2.

Conclusions

Azo dye adsorption on iron, titanium, and aluminum oxides was found to occur via the sulfonic group of the dye-forming bidentate bridging complex with α-Fe_2O_3

(37) Varsany, G.; Lang, L. In *Assignment for Vibrational Spectra of Seven Hundred Benzene Derivatives*; Adam Holger, Ed.; U.K., 1974.

oxides. The ligand exchange with α-FeOOH and TiO_2 leads to unidentate complex formation. Surface complex formation is highly affected by the pH of the solution where acidic pH favors the bond formation. The adsorption at basic pH values is prevented by repulsive electrostatic forces. However, once the electrostatic potential barrier is overcomed, azo dyes are capable of irreversible bond formation. The presence of a small amount of $TiOH_2^+$ below pH 7 was observed to be necessary for the adsorption of the dye on anatase and rutile. The adsorption of Orange II, Orange I, and Orange G was observed to be influenced by the positions of the molecular structure of the dye (available sulfonic groups). The sulfonic group in the benzene ring favors the dye adsorption of Orange I and Orange II. Adsorption of azo dye was less favored when the sulfonic group was on the naphthalene ring, as in the case of Orange G. The latter observations imply a surface molecular recognition mechanism active during the adsorption process. In effect, a crystalline face and a suitable metal−metal atomic distance rather than density of surface sites (surface area) were seen to control the extent of the adsorption. The crystalline face of the oxide with a metal−metal distance close to the sulfo−oxygen atomic distance was found to be optimal for adsorption. This explained why Orange II shows a higher adsorption on α-Fe_2O_3 than on α-FeOOH, TiO_2, and Al_2O_3 oxides.

Acknowledgment. We thank S. Hug of EAWAG for his help during the installation of the programs used in this study. This work was supported by the European Communities Environmental Program ENV-CT 95-0064 (OFES Contract No. 96.350, Bern). We thank Dr. Odile Barres for her valuable help with recording the infrared spectra.

LA9900270